Remote Sensing of Environment 230 (2019) 111201

Contents lists available at ScienceDirect

Remote Sensing of Environment

journal homepage: www.elsevier.com/locate/rse

Satellite data-driven modeling of field scale evapotranspiration in croplands using the MOD16 algorithm framework

Mingzhu He[a,*], John S. Kimball[a,b], Yonghong Yi[c], Steven W. Running[a], Kaiyu Guan[d], Alvaro Moreno[a], Xiaocui Wu[e], Marco Maneta[f]

[a] Numerical Terradynamic Simulation Group, College of Forestry & Conservation, University of Montana, Missoula, MT 59812, USA
[b] Department of Ecosystem and Conservation Sciences, College of Forestry & Conservation, University of Montana, Missoula, MT 59812, USA
[c] Jet Propulsion Laboratory, California Institute of Technology, 4800 Oak Grove Drive, Pasadena, CA 91109, USA
[d] Department of Natural Resources and Environmental Sciences, National Center for Supercomputing Applications, University of Illinois at Urbana- Champaign, Urbana, IL 61801, USA
[e] Department of Microbiology and Plant Biology, Center for Spatial Analysis, University of Oklahoma, Norman, OK 73019, USA
[f] Department of Geosciences, University of Montana, Missoula, MT 59812, USA

ARTICLE INFO

Edited by Emilio Chuvieco

Keywords:
Cropland
Evapotranspiration
30-m
Landsat
MODIS

ABSTRACT

Evapotranspiration (ET) is a key variable linking the global water, carbon and energy cycles, while accurate ET estimates are crucial for understanding cropland water use in context with agricultural management. Satellite remote sensing provides spatially and temporally continuous information that can be used for global ET estimation. The NASA MODIS MOD16A2 operational product provides 500-m 8-day global ET estimates extending from 2001 to present. However, reliable estimates for delineating field level cropland ET patterns are lacking. In this investigation, we modified the MOD16 global algorithm to better represent cropland ET by calibrating model parameters according to C3 and C4 crop types, and incorporating finer scale satellite vegetation inputs to derive 30-m cropland ET estimates over the continental USA (CONUS). Similar overlapping enhanced vegetation index (EVI) records from Landsat and MODIS were used to generate a continuous 30-m 8-day fused EVI and ET record extending from 2008 to 2017 over CONUS croplands. The satellite-based ET estimates were compared with tower based ET observations over different crop types, and more traditional cropland actual ET (AET) estimates derived from reference ET and crop-specific coefficients. The new satellite based 30-m cropland ET estimates (ET_{30m}) corresponded favorably with both tower ET observations (ET_{flux}; $R^2 = 0.69$, RMSE = 0.70 mm d^{-1}, bias = 0.04 mm d^{-1}) and the baseline global MOD16A2 ET product (ET_{MOD16}). The ET_{30m} results also showed better performance against the ET_{flux} observations than ET_{MOD16} ($R^2 = 0.54$, RMSE = 0.82 mm d^{-1}) or AET ($R^2 = 0.52$, RMSE = 2.47 mm d^{-1}) for monitoring CONUS croplands. The spatial and temporal patterns of the ET_{30m} results show enhanced delineation of agricultural water use, including impacts from variable climate, cropland area and diversity. The resulting ET_{30m} record is suitable for operational applications promoting more effective agricultural water management and food security.

1. Introduction

Evapotranspiration (ET) is the loss of water from land surface evaporation (soil and plant surface) and vegetation transpiration, representing the primary link between terrestrial water, energy, and carbon cycles (Allen et al., 2007a; Anderson et al., 2008; Mu et al., 2007; Xiong et al., 2015; Yang et al., 2013). ET is a major hydrological variable in the soil-vegetation-atmosphere system (Senay et al., 2011) and represents approximately 60% of water loss from terrestrial precipitation (Oki and Kanae, 2006). Accurate ET estimates are crucial for understanding local to global water cycle dynamics (Cheng et al., 2011; Nishida et al., 2003), and improving water resource management and drought monitoring (Mu et al., 2013). However, ET is one of the most problematic water cycle elements for effective regional monitoring due to uncertainty contributed from land surface heterogeneity and environmental controls (Mu et al., 2007; Senay et al., 2011; Xu and Singh, 2005).

Several methods have been proposed in recent decades to estimate ET from available ground measurements (Allen et al., 2011), such as the eddy covariance technique (Baldocchi, 2003) and Bowen ratio method

* Corresponding author.
E-mail address: mingzhu.he@ntsg.umt.edu (M. He).

https://doi.org/10.1016/j.rse.2019.05.020
Received 1 December 2018; Received in revised form 19 April 2019; Accepted 14 May 2019
Available online 22 May 2019
0034-4257/

(Scott et al., 2006). However, the general effectiveness of these approaches are restricted to homogeneous sampling areas of approximately 1 km^2, while the available instrumentation and measurement networks are costly and sparsely distributed. Alternatively, satellite remote sensing provides spatially and temporally continuous environmental information that can be used for ET estimation over local to global extents (Allen et al., 2007a, 2007b, 2011; Mu et al., 2007, 2011; Mueller et al., 2013, 2011). The Atmosphere-Land Exchange Inverse (ALEXI) model was developed for mapping ET and soil moisture stress with minimal inputs from ancillary meteorological data while maintaining a physically realistic representation of land-atmosphere exchange over diverse vegetation conditions (Anderson et al., 2007a, 2007b, 2011). Gowda et al. (2009) used a Simplified Surface Energy Balance (SSEB) approach with Landsat TM spectral imagery to estimate ET regionally at fine spatial resolution (30-m) suitable for water resource management (Senay et al., 2011). A global monthly 0.5° resolution land ET record was developed by Jung et al. (2010) using a machine learning empirical model upscaling approach driven by in situ tower site observations (FLUXNET), satellite and surface meteorological data. Zhang et al. (2010) developed a satellite NDVI (normalized difference vegetation index) based ET algorithm using both Penman-Monteith and Priestley-Taylor approaches to assess global terrestrial ET. Allen et al. (2007a, 2007b) introduced the satellite-based METRIC (mapping ET at high resolution with internalized calibration) model, which computes ET as a residual of the surface energy balance, while benefiting from the use of reference conditions for estimating instantaneous ET. METRIC also has advantages of using the surface energy balance to determine ET, since the energy balance can detect reduced ET caused by water shortage, salinity or frost that may not correlate with changes in vegetation cover (Allen et al., 2013). Fisher et al. (2008) used NOAA AVHRR (Advanced Very High Resolution Radiometer) spectral data to estimate global ET using a modified Priestley-Taylor method, calculating ET as the sum of canopy transpiration and evaporation from soil, and canopy intercepted water. The Breathing Earth System Simulator (BESS) is a simplified process-based model coupling atmosphere and canopy radiative transfer, canopy transpiration, photosynthesis and the energy balance, providing a 1-km resolution global ET product from 2000 to 2015 (Jiang and Ryu, 2016). All of these satellite based approaches can provide accurate geospatial ET information, though the utility and reliability of these data are strongly influenced by the quality of the remote sensing data, including sensor spatial and temporal coverage, and signal-to-noise.

The MODIS (Moderate Resolution Imaging Spectroradiometer) sensors on the NASA EOS Terra and Aqua satellites currently provide the only global operational ET product (MOD16A2), which is available at 500-m resolution and 8-day fidelity from 2000 to present (Mu et al., 2007, 2011). The MOD16 ET algorithm is the basis of the MOD16A2 operational product. In the MOD16 algorithm, terrestrial ET is calculated using a modified Penman-Monteith equation as the sum of evaporation from wet and moist soil, evaporation from wet canopy and plant transpiration through canopy stomata. The MOD16 ET record was previously validated against daily and monthly ET observations from a network of global flux tower sites and basin scale water balance calculations, and showed favorable performance (Jung et al., 2010; Mu et al., 2011; Velpuri et al., 2013). These studies indicate general MOD16 ET consistency and utility for local, regional and global scale assessments.

However, uncertainty in the ET estimates from different models can range from 5 to 50% (Morton et al., 2013; Mu et al., 2007), while the MOD16 ET product produced mean uncertainties of 50–60% in monthly ET estimates from several tower observation sites. MOD16 shows a general underestimation of ET in Continental U.S. (CONUS) croplands, which was attributed to model parameterization uncertainty and lack of spatial heterogeneity due to the coarse MODIS footprint (Velpuri et al., 2013; Vinukollu et al., 2011). The MOD16 algorithm also showed an apparent 10 $W m^{-2}$ overestimation of latent energy from 34 global cropland flux towers (Feng et al., 2017), which may reflect model parameterization uncertainty for croplands. Khan et al. (2018) reported generally low agreement (R^2 = 0.35) and positive bias (0.22 mm 8-day^{-1}) between MOD16 and in-situ ET measurements for three rice paddy sites in Asia, which was attributed to local vegetation and microclimate variability missing from the global land cover classification and spatially coarse (~ 0.5-degree) resolution GMAO meteorological data used as model drivers. Vapor pressure deficit (VPD) derived from the coarse GMAO meteorological data may not adequately reflect water stress conditions over smaller sub-regions, contributing additional uncertainties to the MOD16A2 ET product (Wang et al., 2015). Therefore, further refinements to the MOD16 framework are needed to better represent field level vegetation and meteorological conditions influencing ET and associated water use conditions in croplands.

Traditionally, ET in croplands is calculated as the product of crop-specific empirical coefficients multiplied by a reference ET rate, which has been the standard approach for cropland ET calculations in the United States for > 40 years (Allen et al., 2005, 2007a; Tasumi and Allen, 2007). Reference ET (ET_{ref}) is the rate at which available water is vaporized from a reference vegetated surface (alfalfa or grass) where water is non-limiting (Jensen et al., 1990). Here, ET_{ref} defines the potential upper bound of evapotranspiration under variable climate conditions using a fixed vegetation reference (alfalfa), while an empirical crop coefficient (Kc) is used with ET_{ref} to derive an estimate of actual ET (AET) for different crop types. The Kc value is generally determined for different crop types and growth stages ranging from emergence to termination. However, the assigned Kc values may not represent actual vegetation and growing conditions of different crops, especially in water limited areas (Allen et al., 2007b). Kc values generally cannot extend beyond about 1.0–1.05 times the reference condition, but may actually be up to 1.1 times the reference condition in arid and semi-arid regions for a given crop type (Allen et al., 2011); this uncertainty makes it difficult to predict the actual Kc over large regions with variable climate.

The objective of this study is to improve the delineation of field scale (30-m) cropland ET dynamics over the CONUS domain using a satellite-based modeling framework that builds on the MOD16 ET algorithm logic. A modified version of the MOD16 algorithm is used in this study to estimate cropland ET at 30-m and 8-day resolution spanning the CONUS domain and recent satellite record (2008–2017). Annual variations in crop type and area are defined using the 30-m Cropland Data Layer (CDL) from the U.S. Department of Agriculture (USDA) National Agricultural Statistics Service (NASS). A continuous 30-m 8-day Enhanced Vegetation Index (EVI) record is generated by fusing 30-m EVI records from Landsat 5 and 7, with similar but coarser resolution MODIS EVI observations. The fused EVI record is used to define canopy cover and ET partitioning between evaporation and transpiration in the ET algorithm. A 4-km CONUS surface meteorology record is used to provide daily meteorological inputs to the ET model, which is calibrated to distinguish C3 and C4 crop types and validated against flux tower-based daily ET observations from seven CONUS cropland sites. The model results are also compared with the operational MODIS MOD16A2 (version 6) global ET product and ET_{ref} and AET estimates for different CONUS cropland areas over the multi-year study period. The estimated 30-m ET results are examined over two selected sub-regions with different climate and cropland conditions to document potential model improvements in representing field-level ET patterns and seasonal to inter-annual variability over heterogeneous croplands. These results provide a new regional data record for documenting cropland ET trends, with suitable accuracy and performance for water resource assessment and monitoring applications.

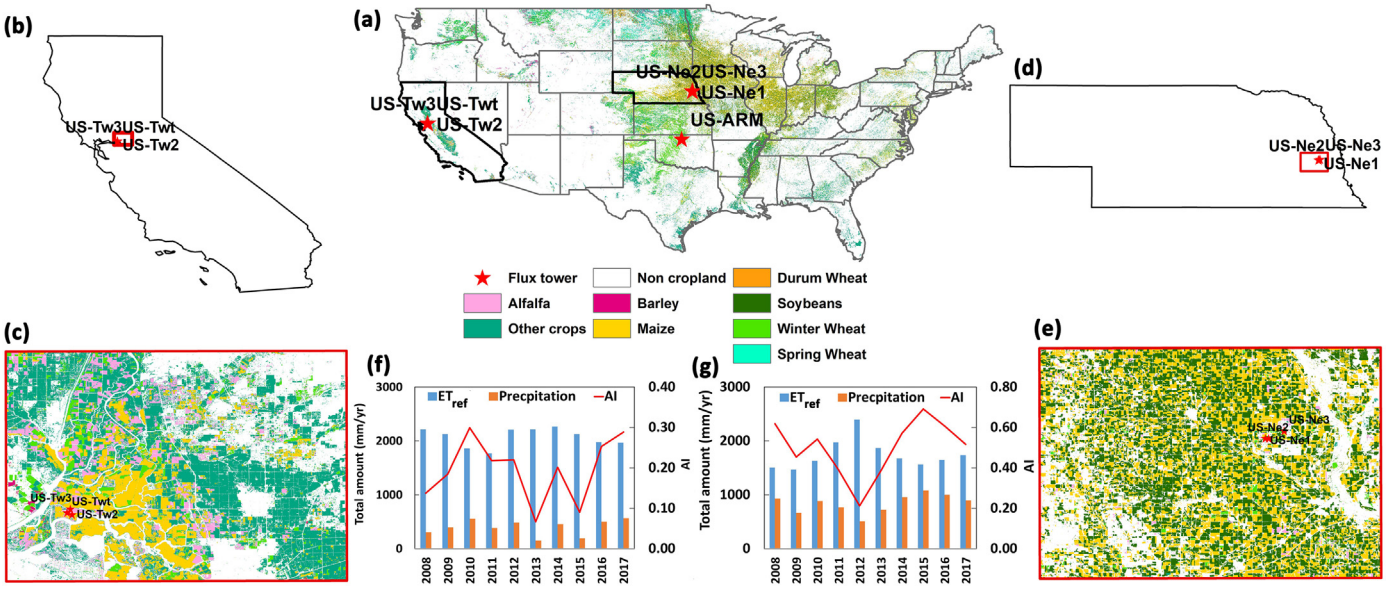

Fig. 1. Cropland distributions across the CONUS domain in 2008 (a); locations of two regions of interest centered over flux tower sites in (b) California (ROI1) and (c) Nebraska (ROI2); 30 m cropland patterns over ROI1 (d) and ROI2 (e) are also shown, along with variations of mean annual precipitation, reference ET (ET_{ref}) and climate aridity index (AI) during 2008–2017 for the ROI1 (f) and ROI2 (g) sub-regions. The AI classifications represent: hyper-arid ($AI < 0.05$), arid ($0.05 \leq AI < 0.20$), semi-arid ($0.20 \leq AI < 0.5$), sub-humid ($0.50 \leq AI \leq 0.65$), and humid ($AI > 0.65$) categories.

2. Materials and methods

2.1. Study domain

The domain for this investigation encompasses CONUS cropland areas from 2008 to 2017. The USDA NASS CDL provides dynamic annual cropland distribution information at 30-m resolution over the CONUS domain from 2008 to present. The CDL reported total cropland area shows a significant increasing trend ($r = 0.85$; $p < 0.05$), ranging from 1.32 * 10^8 ha (2010) to 1.42 * 10^8 ha (2017), and accounting for about 17% ~ 18% of the total CONUS land area from 2008 to 2017. The CDL captures substantial variability in cropland type and area over the study period that reflects changes in underlying vegetation, land use and management practices, which are expected to strongly influence ET.

The CONUS CDL cropland classification in 2008 is shown in Fig. 1. Croplands are mainly distributed in the CONUS midwest, southwest, northwest and southern areas (Fig. 1a). There are seven available flux tower sites representing different crop types within the domain (Fig. 1a), which are summarized in Table 1; these sites provide eddy covariance flux measurements and supporting meteorological data for the study period obtained from the FLUXNET2015 record, including latent heat flux measurements used to obtain tower daily ET observations (ET_{flux}). Three of the tower sites (US-Tw2, US-Tw3 and US-Twt) are located in California (Fig. 1b); three other tower sites (US-Ne1, US-Ne2, and US-Ne3) are located in Nebraska (Fig. 1c), and the remaining tower site (US-ARM) is located in Oklahoma (Fig. 1a). The crop types represented by the tower sites include maize, soybean, winter wheat, rice and alfalfa (Table 1), which vary across sites and also over the study period at some sites due to crop rotation practices.

The cropland ET is simulated at 30-m resolution in this investigation, resulting in a very large (> 12 TB) CONUS cropland ET data record for the 2008 to 2017 period. Thus, two sub-regions (Fig. 1b, c), each representing about 50-km x 75-km, were selected for more intensive investigations of cropland heterogeneity. The sub-regions were delineated around selected tower sites in California and Nebraska representing different climate, crop type and management conditions. The Aridity Index (AI), calculated as the ratio of annual precipitation to ET_{ref}, is used as an indicator of climate dryness (UNESCO, 1979) in each sub-region, including hyper-arid ($AI < 0.05$), arid ($0.05 \leq AI < 0.20$), semi-arid ($0.20 \leq AI < 0.5$), sub-humid ($0.50 \leq AI \leq 0.65$), and humid ($AI > 0.65$) conditions. The California region of interest (ROI1) has annual precipitation of 399 ± 145 mm yr^{-1} over the 2008–2017 record (Fig. 1f), while ET_{ref} is much higher than the annual precipitation in this region, leading to a very low AI (0.20 ± 0.08) and indicating that ROI1 is water-limited. The estimated AI in 2013 and 2015 was only 0.07 and 0.09, respectively, suggesting very dry conditions in ROI1. The major ROI1 crop types include maize, alfalfa, and winter wheat during the study period (Fig. 1d). In contrast, the Nebraska region (ROI2) has much higher annual precipitation (841 ± 173 mm yr^{-1}) than ROI1, with semi-arid or sub-humid AI conditions for most of the study period (AI = 0.53 ± 0.10), except for particularly dry conditions in 2012 (AI = 0.21) (Fig. 1g). The dominant ROI2 crops are maize, soybean, winter wheat and alfalfa over the study period. Both sub-regions show

Table 1
Summary of the seven CONUS cropland flux tower sites used in this study.

Tower site	Latitude	Longitude	Date period	Crop	Reference
US-ARM	36.6058	−97.4888	2008–2012	Maize, winter wheat	Fischer et al. (2007)
US-Ne1	41.1651	−96.4766	2008–2012	Maize, soybean	Suyker et al. (2005)
US-Ne2	41.1649	−96.4701	2008–2012	Maize, soybean	Suyker et al. (2004)
US-Ne3	41.1797	−96.4397	2008–2012	Maize, soybean	Suyker et al. (2004)
US-Tw2	38.1047	−121.643	2012–2013	Maize	Knox et al. (2015)
US-Tw3	38.1159	−121.647	2013–2014	Alfalfa	Oikawa et al. (2017)
US-Twt	38.1087	−121.653	2009–2014	Rice	Baldocchi et al. (2016)

contrasting climate and crop conditions encompassing the general range of CONUS cropland and ET variability.

2.2. MOD16 ET algorithm

The MOD16 ET algorithm (Mu et al., 2011, 2007) is based on the well-known Penman-Monteith equation (Eq. (1)). The algorithm calculates evaporation from the soil and wet canopy, along with plant transpiration, while the ET is derived as the daily sum of these components. A detailed description of the MOD16 algorithm is provided by (Mu et al., 2011), and summarized below.

$$\lambda E = \frac{s * A + \rho * C_p * VPD/r_a}{s + \gamma * (1 + r_s/r_a)} \quad (1)$$

Where λE is the latent energy of ET ($W\,m^{-2}$), which can be converted to water units (mm d^{-1}) based on the temperature (T; °C) dependent latent heat of vaporization (λ, J kg^{-1}) and the assumption that the ET rate varies conservatively over a diurnal cycle; $s = d(e_{sat})/dT$, which is the slope of the curve of saturated water vapor pressure (e_{sat}) to T. A ($W\,m^{-2}$) is the daily total available solar energy at the land surface. VPD (Pa) is the mean daytime atmospheric vapor pressure deficit. r_s ($s\,m^{-1}$) and r_a ($s\,m^{-1}$) are the surface and aerodynamic resistances to evaporation, respectively, which are among the most important variables in the algorithm, especially in calculating transpiration (Mu et al., 2011). In the plant transpiration process, r_s represents the surface resistance to canopy transpiration, which is equivalent to the inverse of canopy conductance (C_c), and calculated as follows (Mu et al., 2011).

$$G_s^1 = C_L * m(Tmin) * m(VPD) * r_{corr} \quad (2)$$

$$r_{corr} = \frac{1}{\frac{101300}{P_a} * \left(\frac{T_l + 273.15}{293.15}\right)^{1.75}} \quad (3)$$

$$m(T_{min}) = \begin{cases} 1 & T_{min} \geq T_{\min open} \\ \frac{T_{min} - T_{\min close}}{T_{\min open} - T_{\min close}} & T_{\min close} < T_{min} < T_{\min open} \\ 0 & T_{min} \leq T_{\min close} \end{cases} \quad (4)$$

$$m(VPD) = \begin{cases} 1 & VPD \leq VPD_{open} \\ \frac{VPD_{close} - VPD}{VPD_{close} - VPD_{open}} & VPD_{open} < VPD < VPD_{close} \\ 0 & VPD \geq VPD_{close} \end{cases} \quad (5)$$

$$C_c = \begin{cases} \frac{G_s^2 * (G_s^1 + G_{CU})}{G_s^1 + G_s^2 + G_{CU}} * LAI * (1.0 - Fwet) & (LAI > 0, (1 - F_{wet}) > 0) \\ 0 & (LAI = 0, (1 - F_{wet}) = 0) \end{cases} \quad (6)$$

$$G_{cu} = g_{cu} * r_{corr} \quad (7)$$

$$G_s^2 = gl_{sh} \quad (8)$$

$$r_s = \frac{1}{C_c} \quad (9)$$

Stomatal conductance ($G_s{}^1$, m s^{-1}) is constrained by dimensionless scalars ranging between 0 (fully constrained) and 1 (no constraint) for VPD ($m(VPD)$) and daily minimum air temperature ($m(T_{min})$), corrected by the function, r_{corr}, indicating stomatal conductance variations with air temperature and atmospheric water demands. P_a (Pa) is the atmospheric pressure, calculated as a function of elevation. G_{cu} (m s^{-1}) is the leaf cuticular conductance, while $G_s{}^2$ (m s^{-1}) is the leaf boundary-layer conductance, and g_{cu} is the leaf conductance per unit leaf area index (LAI, $m^2\,m^{-2}$), prescribed as a constant (0.00001 m s^{-1}). $Fwet$ is the water cover fraction within a grid cell, estimated from the relative humidity. All of the parameters (C_L, $T_{\min open}$, $T_{\min close}$, VPD_{open}, VPD_{close}, gl_{sh}) in Eqs. (2)–(9) are vegetation-specific, and defined from a global Biome Property Look Up Table (BPLUT) in the MODIS MOD16A2 operational product (Running et al., 2018), where the BPLUT only defines a single cropland biome type.

In this study, we developed a more detailed MOD16 BPLUT calibration and parameterization that distinguishes C3 and C4 crop types for estimating ET. Model simulations were conducted using both the original BPLUT representing a single global crop type (Running et al., 2018) and the new BPLUT C3 and C4 crop type parameterizations to clarify the impact of the more detailed crop type delineation on model ET performance. Approximately 30 site-years of observations from seven CONUS cropland flux tower sites were used for model calibration and validation. The tower site records included 18 site-years representing C4 crops (maize) and 12 other site-years representing C3 crops, including soybean, winter wheat, rice and alfalfa. The sensitivity of the major MOD16 BPLUT parameters were checked against tower observations at each of the seven cropland tower sites. The model sensitivity results indicated that C_L, VPD_{close}, and VPD_{open} (Eqs. (2) and (5)), used for calculating the surface resistance to plant transpiration, were the three most sensitive parameters in simulating cropland ET (results not shown). The Markov Chain Monte Carlo (MCMC) method was used for simultaneous iterative calibration of the three model parameters (Table 2) by minimizing the root mean square error (RMSE) between model ET calculations and ET_{flux}. The model BPLUT calibration was conducted separately for C3 and C4 crop types. Two-thirds of the tower based ET estimates were randomly selected for model calibration, while all available tower observations were used for model ET validation.

Several different ET model scenarios were used in this study and summarized in Table 3. ET_{sim} is the 30-m cropland ET derived from the MOD16 ET algorithm using the original BPLUT, while ET_{30m} represents the 30-m cropland ET calculated from MOD16 ET algorithm with the updated BPLUT representing both C3 and C4 crops. Both ET_{30m} and ET_{sim} use the same 30-m vegetation and 4-km daily surface meteorology inputs (described below), which provide 12–16-fold resolution enhancement over the MOD16A2 operational ET product.

In this study, all of the data including model inputs and MODIS products are converted to a consistent geographic projection and WGS84 datum. Daily meteorological data are used as key model drivers, including shortwave solar radiation, surface air temperature, VPD and relative humidity. The MOD16A2 operational product uses daily surface meteorology inputs from the ~ 0.5° resolution NASA Global Modeling and Assimilation Office (GMAO) product (Schubert et al., 1993). In this study we used a finer resolution (4-km) CONUS daily surface meteorology record from the University of Idaho Gridded Surface Meteorological dataset (Gridmet; Abatzoglou, 2013). The ET model calculations in this study were conducted on a daily basis for each 30-m cropland grid cell defined from the annual CDL land cover record and fused Landsat-MODIS EVI record (described below). The MODIS daily 500-m global albedo product (MCD43A3 v6; Schaaf and Wang, 2015) was used to derive the available surface solar radiation. The resulting model daily ET calculations were then averaged over a coarser 8-day time step for each grid cell, consistent with the MOD16A2 ET record.

The estimated 30-m 8-day ET record from this study was compared against the 500-m 8-day MODIS MOD16A2 (v6) ET product (ET_{MOD16}) over the CONUS cropland domain and 2008–2017 study period. The MODIS annual 500-m land cover product (MCD12Q1 Type 2; Friedl and

Table 2
The calibrated parameters used in this study for C3 and C4 crops.

Crop type	VPD_{close} (pa)	VPD_{open} (pa)	C_L (m s^{-1})
C3	4347	804	0.014
C4	4575	885	0.016

Table 3
Descriptions of different ET estimates included in this study.

Terminology	Description	Resolution
ET_{flux}	ET estimates derived from tower latent heat flux observations	Site-level, 8-day
ET_{MOD16}	MODIS MOD16A2 global operational ET product (version 6)	500-m, 8-day
ET_{sim}	Cropland ET estimates derived from MOD16 ET algorithm with the original BPLUT	30-m, 8-day
ET_{30m}	Cropland ET estimates derived from MOD16 ET algorithm with the calibrated parameters distinguishing C3 and C4 crops	30-m, 8-day
ET_{ref}	Reference ET derived from Eq. 11, defining the potential upper bound of ET under variable climate conditions	4-km, 8-day
AET	Cropland actual ET derived from ET_{ref} and crop coefficients (Kc) in Eq. 12	30-m, 8-day

Sulla-Menashe, 2015) is used in this study to characterize cropland in the ET_{MOD16} product. Since the MCD12Q1 land cover product only extends to 2016, we used the 2016 land cover information to represent 2017, assuming no obvious land cover changes between the two years.

2.3. Generating 30-m 8-day Landsat-MODIS fused EVI data for CONUS over 2008–2017

In the original MOD16 algorithm logic, EVI is used for estimating the vegetation canopy cover fraction (*Fc*; Eq. (10)) for partitioning net radiation between the canopy and soil surface (Mu et al., 2007).

$$Fc = \frac{EVI - EVI_{\min}}{EVI_{max} - EVI_{min}} \tag{10}$$

where EVI_{min} and EVI_{max} are the minimum and maximum EVI during the study period, respectively. In the current study, a pixel-wise linear regression model is developed to generate a 30-m 8-day EVI record to calculate Fc for the cropland ET calculations. The 30-m EVI record was derived by empirically fusing similar overlapping EVI records from MODIS and Landsat (5 and 7) over CONUS croplands using the Google Earth Engine (GEE) platform, which includes extensive geospatial data libraries and provides efficient and fast calculations involving very large datasets. The 30-m surface reflectance data for bands 1 (blue), 3 (red) and 4 (near infrared) from Landsat 5 and 7 had a 16-day revisit interval, and were processed to screen out cloud-contaminated pixels. The remaining clear-sky spectral data were used to derive the Landsat 30-m EVI record (Huete et al., 1997). Similar surface reflectance data for bands 1 (red), 2 (near infrared), and 3 (blue) from the 500-m 8-day MODIS surface reflectance product (MOD09A1 v6; Vermote, 2015) were also extracted and screened for cloud-contaminated pixels to calculate the coarser resolution MODIS EVI record. Since MODIS and Landsat provide similar spectral vegetation information for the same region and time period, we assumed that the overlapping EVI retrievals from these sensors are consistent and comparable. We therefore developed a pixel-wise linear regression model describing relationships between Landsat and MODIS EVI retrievals for each year of record following a similar approach developed for estimating CONUS cropland productivity (He et al., 2018). The resulting models were then used to generate a continuous 30-m 8-day EVI product for the CONUS domain from 2008 to 2017, which was used as a model input to derive cropland ET simulations at the same scale using the MOD16 framework.

2.4. Cropland reference ET and actual ET calculations

The standardization of the ET_{ref} calculation (Eq. (11); Allen et al., 2005), as recommended by the Task Committee on Standardization of Reference Evapotranspiration of the ASCE-EWRI, is simplified from the Penman-Monteith equation (Eq. (1)):

$$ET_{ref} = \frac{0.408s(R_n - G) + \gamma\frac{C_n}{T+273}u_2 VPD}{s + \gamma(1 + C_d u_2)} \tag{11}$$

where s is the slope of saturation vapor pressure-temperature curve (kPa °C^{-1}); R_n is the net solar radiation at the crop surface (MJ m^{-2} d^{-1}); G is the soil heat flux density (MJ m^{-2} d^{-1}); γ is the psychrometric constant (kPa °C^{-1}); C_n and C_d (K mm s^3 Mg^{-1} d^{-1}) are constant values based different reference vegetation surfaces (grass and alfalfa); T (°C) is the mean daily air temperature at 1.5 to 2.5 m height; u_2 (m s^{-1}) is the mean daily wind speed at 2 m height; and *VPD* (kPa) is the vapor pressure deficit at 1.5 to 2.5 m height (Allen et al., 2005).

Here, ET_{ref} (mm d^{-1}) is derived for an alfalfa reference condition at a daily time step using the 4-km Gridmet meteorological data from 2008 to 2017 across the CONUS domain. Empirical crop coefficients (Kc) are incorporated to estimate actual cropland ET (AET) from ET_{ref} using the following equation.

$$AET = ET_{ref} * Kc \tag{12}$$

Kc represents the ratio of AET to ET_{ref} for different crop types and growth stages, while Kc values for the major CONUS crop types were obtained from the US Bureau of Reclamation's AgriMet program (https://www.usbr.gov/pn/agrimet/cropcurves/crop_curves.html). The Kc values were spatially applied to the 4-km ET_{ref} calculations to derive 30-m AET over the CONUS croplands and 2008–2017 study period, where annual crop type and cropland area were defined from the USDA NASS CDL. The AET results were then used with the other ET metrics (ET_{MOD16}, ET_{sim}, ET_{flux}) for validating the ET_{30m} record.

2.5. Statistical metrics

In this study, the ET estimates, including ET_{MOD16}, ET_{sim}, ET_{30m} and AET, were extracted as spatial mean values within a 1-km by 1-km window centered over each tower site, which is similar to the tower observation footprint (Baldocchi et al., 2001), and compared with the associated tower ET_{flux} observation. However, the 4-km ET_{ref} was extracted from the same locations as the tower observations. Model performance was evaluated using the coefficient of determination (R^2), RMSE and bias between the model ET estimates (ET_{sim}, ET_{MOD16}, ET_{30m}, ET_{ref} and AET) and the corresponding tower ET_{flux} observations. The RMSE and bias were expressed as relative percentages of ET_{flux} for the model assessment. Pearson's correlation coefficient (r) was also used to evaluate the sign and strength of the relationships between the model ET estimates and selected climate variables, where significant relationships were assessed at the 95% significance threshold (p-value ≤ 0.05).

3. Results

3.1. CONUS cropland 30-m ET simulations

The ET_{MOD16} record shows relatively good correspondence with ET_{flux} for both C3 and C4 crop types represented at the seven CONUS tower sites examined (Fig. 2, Table 4). In this study, the ET model performance was evaluated at the 8-day time step consistent with the MOD16A2 operational ET product, while the daily model ET results (not shown) were found to be consistent with the coarser averaged 8-day results. For all of the cropland tower sites, ET_{MOD16} explains about 54% of the variability in the ET_{flux} observations, but with large uncertainty (62% ≤ relative RMSE ≤63%; Table 4), and general overestimation (9% ≤ bias ≤15%) compared with ET_{flux}. The ET_{sim} results show stronger correspondence with ET_{flux} than ET_{MOD16}, with

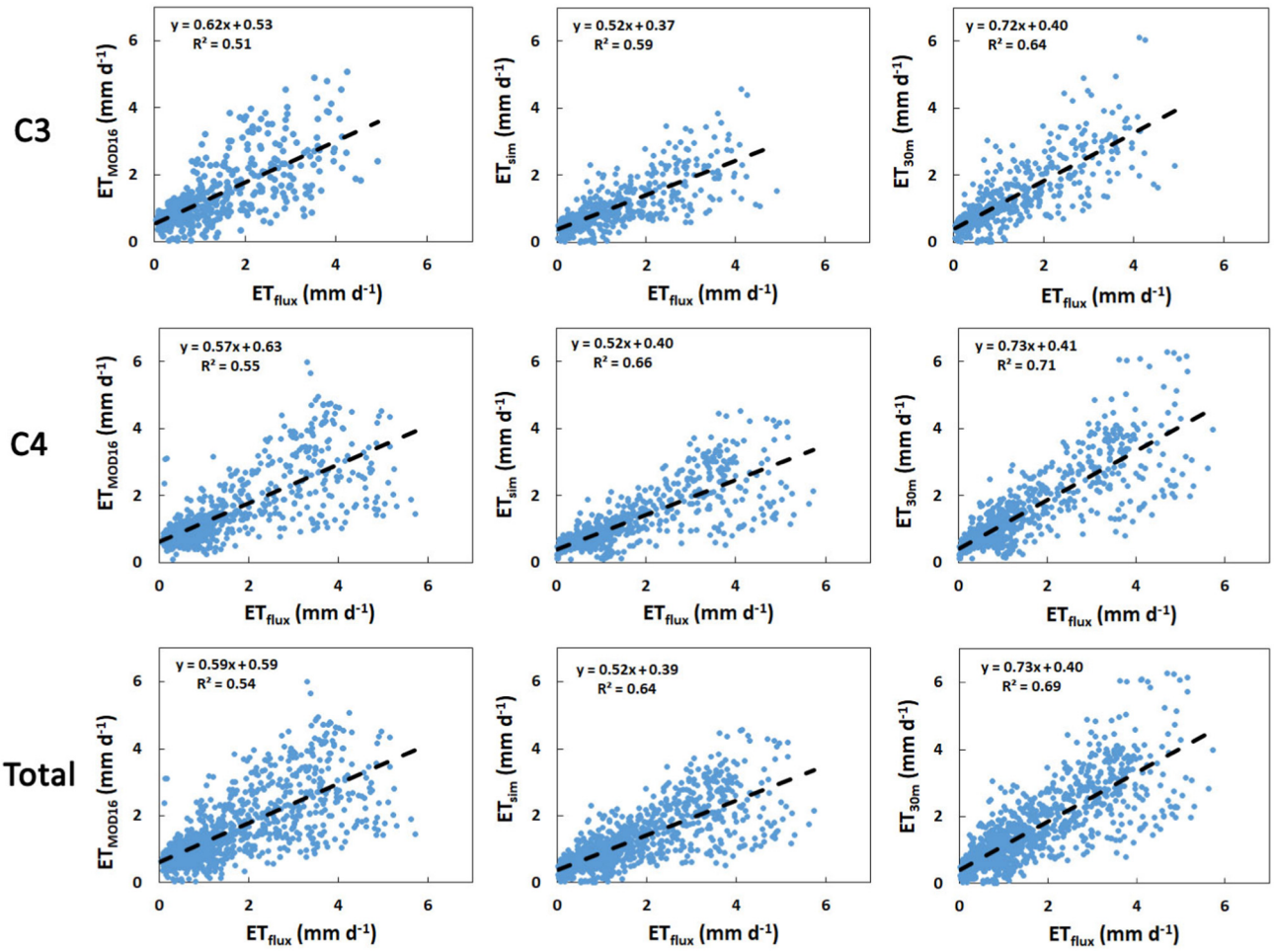

Fig. 2. Comparisons between flux tower based ET observations (ET_{flux}) and corresponding ET estimates from the MODIS MOD16A2 (v6) 500-m 8-day operational product (ET_{MOD16}); finer 30-m ET estimates derived using the MOD16 ET algorithm with original BPLUT (ET_{sim}), and the new BPLUT with calibrated C3 and C4 cropland parameters (ET_{30m}). The models are evaluated against tower ET observations (ET_{flux}) at seven cropland sites representing different CONUS climate, crop type and management practices.

Table 4
Statistical comparisons between flux tower ET observations (ET_{flux}) and the MODIS operational ET product (ET_{MOD16}), 30-m ET estimates derived using the MOD16 ET algorithm with the original BPLUT (ET_{sim}) and the new calibrated cropland parameters at seven CONUS flux tower sites (ET_{30m}).

Crop type	ET_{MOD16}			ET_{sim}			ET_{30m}		
	R^2	RMSE (mm d^{-1})	Bias (mm d^{-1})	R^2	RMSE (mm d^{-1})	Bias (mm d^{-1})	R^2	RMSE (mm d^{-1})	Bias (mm d^{-1})
C3	0.51	0.75	0.17	0.59	0.73	−0.20	0.64	0.66	0.06
C4	0.55	0.86	0.13	0.66	0.86	−0.27	0.71	0.73	0.03
Total	0.54	0.82	0.15	0.64	0.81	−0.25	0.69	0.70	0.04

approximately 16 to 20% higher R^2 correspondence and slightly reduced RMSE (Table 4). The improved ET_{sim} performance reflects better representation of field scale ET heterogeneity relative to the coarser MOD16A2 record. However, the ET_{sim} results show systematic ET underestimation relative to the ET_{flux} observations, with negative bias of −0.25 mm d^{-1} (−19%) for all crop sites examined (Table 4). These results indicate the potential for further model enhancement through BPLUT calibration refinements that better represent C3 and C4 crop type characteristics.

The ET_{30m} results explain about 64%, 71% and 69% of the variability in the tower ET_{flux} observations for C3, C4 and all crop types represented, respectively (Fig. 2, Table 4). No apparent ET_{30m} bias was found relative to the tower ET_{flux} observations at these sites (Table 4). Moreover, the ET_{30m} results show 26% ~ 29% (8% ~ 9%) stronger correspondence and 12% ~ 16% (10% ~ 16%) lower RMSE than the ET_{MOD16} (ET_{sim}) results relative to ET_{flux}. These results indicate improved ET_{30m} accuracy and performance in representing both field scale cropland ET dynamics and crop type differences across the CONUS tower sites. The ET_{30m} results show marked accuracy and performance enhancement over ET_{MOD16} that reflect the advantages of finer 30-m model land cover (CDL) and vegetation (EVI) inputs, and the improved resolution (4-km) of the Gridmet meteorological inputs relative to the global baseline. Unlike ET_{MOD16} and ET_{sim}, the ET_{30m} results also benefit from a refined model BPLUT that distinguishes C3 and C4 crop types (Table 2). Overall, the ET_{30m} results show generally improved model consistency in representing the observed cropland ET seasonal variability and magnitudes.

The variations of annual cropland ET_{30m} for different crop types in 2008 are shown in Fig. 3. The mean annual cropland ET_{30m} is about 467.46 ± 171 mm yr^{-1} over the study domain in 2008, while C4 crops show approximately 3% larger annual ET_{30m} rates than C3 crops (Fig. 3). Differences in annual ET_{30m} distributions across the five major CONUS crop types (alfalfa, barley, maize, soybean and wheat) are presented in Fig. 3. Maize is one of the major C4 crops and is widely distributed across the domain. Maize also shows 3% ~ 6% larger annual ET_{30m} than the four major C3 crop types (Fig. 3); whereas, barley (C3) shows the smallest annual ET_{30m} (448.29 mm yr^{-1}) among the selected

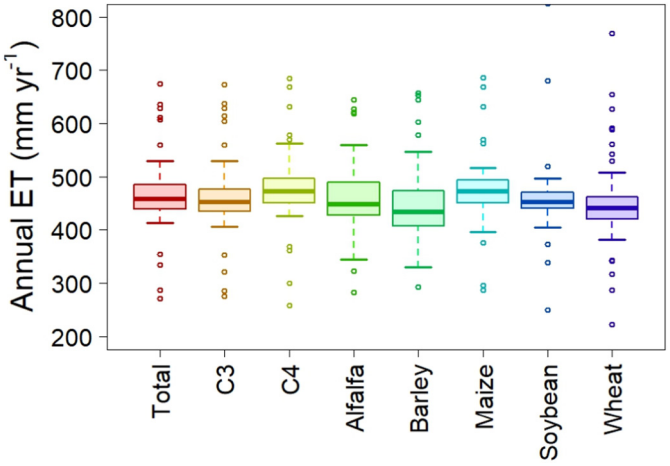

Fig. 3. Dynamics of annual 30-m cropland ET estimates from this study (ET_{30m}) for all CONUS croplands (Total), along with finer delineations for C3, C4, alfalfa, barley, maize, soybean and wheat (spring, winter, and durum) crop types in 2008.

major crops in 2008.

3.2. Site and regional model performance evaluation in California (ROI1)

The California sub-region (ROI1) encompasses three tower sites representing major crop types (alfalfa, maize, winter wheat) under arid to semi-arid climate conditions (AI = 0.20 ± 0.08; Fig. 1f). At the site-level, the ET_{30m} and AET model results were sampled as spatial mean values within 1-km^2 windows centered over each ROI1 tower site and evaluated against collocated ET_{flux} observations representing maize (US-Tw2), alfalfa (US-Tw3), and rice (US-Twt) crop types (Fig. 4); the results were also compared with alternative ET_{MOD16} and ET_{ref} estimates within ROI1 surrounding these tower sites (Fig. 5).

At all three tower sites, ET_{ref}, AET, and ET_{30m} show similar seasonal cycles as ET_{flux}, while ET_{MOD16} shows slightly different seasonal dynamics during the study period (Fig. 4). ET_{ref} and AET are much higher than the ET_{flux} observations and other model results (ET_{MOD16}, ET_{30m}) at all three tower sites, especially during the peak growing season (May to August; Fig. 4); whereas the ET_{30m} and ET_{MOD16} results are similar in magnitude. ET_{30m} shows stronger agreement with the ET_{flux} observations at US-Tw2 (maize) than that at US-Tw3 (alfalfa) and US-Twt (rice) sites, with higher R^2 (0.72) and lower RMSE (0.53 mm d^{-1}) and bias (−0.13 mm d^{-1}) (Fig. 4). AET captures 44% ~ 64% seasonal variations of ET_{flux}, but with large overestimation (69% ~ 161%) of ET_{flux} at the three tower sites. ET_{ref} shows even larger overestimation of ET_{flux} than AET (Fig. 4), with relative bias of 134% ~ 260% at the tower sites; however, ET_{ref} still captures 44% ~ 77% of the ET_{flux} observed temporal variability at these sites. Overall, in terms of seasonal dynamics and magnitude, ET_{30m} shows the best performance against the tower ET_{flux} observations at the three California cropland sites relative to the other ET metrics, including the highest R^2 (0.61), lowest RMSE (0.95 mm d^{-1}) and lowest bias (−0.37 mm d^{-1}).

The regional patterns of mean annual ET from the different models and 2008–2017 study period within ROI1 are presented in Fig. 5. ET_{ref} shows much higher values in this region compared with AET, ET_{MOD16} and ET_{30m}, along with a decreasing west-to-east trend (Fig. 5). The large ET_{ref} magnitude in this region is expected due to the semi-arid climate, which enhances atmospheric moisture holding capacity and potential ET. The AET metric derived from ET_{ref} also shows very high values (≥1100 mm yr^{-1}) in the southwest and northwest portions of the region dominated by maize and alfalfa (Fig. 5b), and relatively low values in the west of ROI1, where winter wheat is the dominant crop. The ET_{MOD16} results show relatively low spatial heterogeneity in the region owing to the coarser resolution vegetation (500-m) and meteorological (~ 0.5°) inputs used in the MOD16A2 global product; however, the ET_{MOD16} results still reveal generally higher ET values in the south, northwest and southeast portions of ROI1 (Fig. 5c). The ET_{30m} results show relatively lower annual ET across ROI1 than the AET and ET_{MOD16} results, but with large spatial heterogeneity (Fig. 5d). The ET_{30m} results also show a strong regional gradient ranging from 500 to 700 mm yr^{-1} in the southern portion of ROI1 composed mainly of maize and alfalfa, to < 200 mm yr^{-1} in the western and northeast portions of the region representing winter wheat (Fig. 5d). The ET_{30m} results also show a strong delineation of ET variability within and across different agricultural fields that are reduced or missing from the coarser ET_{MOD16} product (Fig. 5).

3.3. Spatiotemporal variations of cropland ET from 2008 to 2017 in Nebraska (ROI2)

The ability of the model ET_{30m} record to represent ET variability due to both climate and annual variations in crop type and area is evaluated relative to ET_{MOD16} over the 2008–2017 study period within a selected 50 km × 75 km sub-region in Nebraska (ROI2; Fig. 1c). ROI2 is in the same size as ROI1, and also encompasses three cropland tower sites, but with different climate conditions and crop types represented (Fig. 1e, g). The major ROI2 crop types include maize, soybean and winter wheat, with frequent crop rotations, while the regional climate ranges from semi-arid to sub-humid (AI = 0.53 ± 0.10) with annual precipitation of 841 ± 173 mm yr^{-1} over the 2008–2017 record.

The mean annual ET_{30m} in ROI2 is 327 ± 220 mm yr^{-1} (Fig. 6a) over the study period, though some areas dominated by winter wheat show a lower annual rate (≤ 200 mm yr^{-1}). The ET_{MOD16} record depicts higher ROI2 mean annual values (475 mm yr^{-1}) and lower spatial heterogeneity (78 mm yr^{-1}) than ET_{30m} over the study period (Fig. 6a, c). Similar to the ROI1 results, the ET_{30m} results preserve field level ET patterns better than the coarser ET_{MOD16} record in ROI2, despite differences in cropland characteristics between the two sub-regions.

The ET_{30m} results show both increasing and decreasing ET trends across ROI2 from 2008 to 2017 (Fig. 6b). Specifically, the fluctuation of ET_{30m} over the ten-year study period is relatively small in the central area of ROI2, ranging from −4 to 4 mm yr^{-2} (Fig. 6b). The ET_{30m} results show a decreasing ET trend in the northwest and southeast areas of ROI2, and an increasing ET trend in the western and eastern portions of the region. Areas with small mean annual ET_{30m} (Fig. 6a) generally show an increasing trend (Fig. 6b). In contrast, the ET_{MOD16} record shows a larger and more uniform ET increase (> 10 mm yr^{-2}) over the study period and ROI2 region (Fig. 6d). The largest ET_{MOD16} increase (~ 40 mm yr^{-2}) is shown in the eastern and southwest areas of ROI2 (Fig. 6d), where ET_{30m} also shows a relatively large increasing trend (~ 20 mm yr^{-2}; Fig. 6b). However, the ET_{MOD16} record shows an increasing trend (20–35 mm yr^{-2}) in the southeast area of ROI2, contrasting with a minimal or small decreasing ET_{30m} trend (0 ~ −10 mm yr^{-2}) for the same area.

The spatial mean of annual ET_{30m} for ROI2 ranges from a low in 2014 (415.61 mm yr^{-1}) to a peak in 2012 (635.07 mm yr^{-1}), with no obvious trend over the period of record (Fig. 7a). The spatial mean of annual ET_{MOD16} for ROI2 shows a weak (p = 0.21) increasing trend during the study period, with the smallest value (375.98 mm yr^{-1}) in 2012 (Fig. 7a). 2012 was also the driest year of record (i.e. AI = 0.21) over the 2008–2017 period in this region, indicating greater atmospheric moisture demand and cropland water requirements for this year. Furthermore, the tower ET_{flux} at the three different cropland sites in this region (US-Ne1, US-Ne2 and US-Ne3) all show higher annual ET in 2012 (~ 469.17 mm yr^{-1}) relative to other years of record (2008–2011) ranging from 432.17 to 454.13 mm yr^{-1}. The mean annual ET_{flux} from the three ROI2 tower sites shows a significant decreasing trend (r = −0.73; p < 0.05) with more humid climate conditions (Fig. 8), indicating that crop water demands are higher under

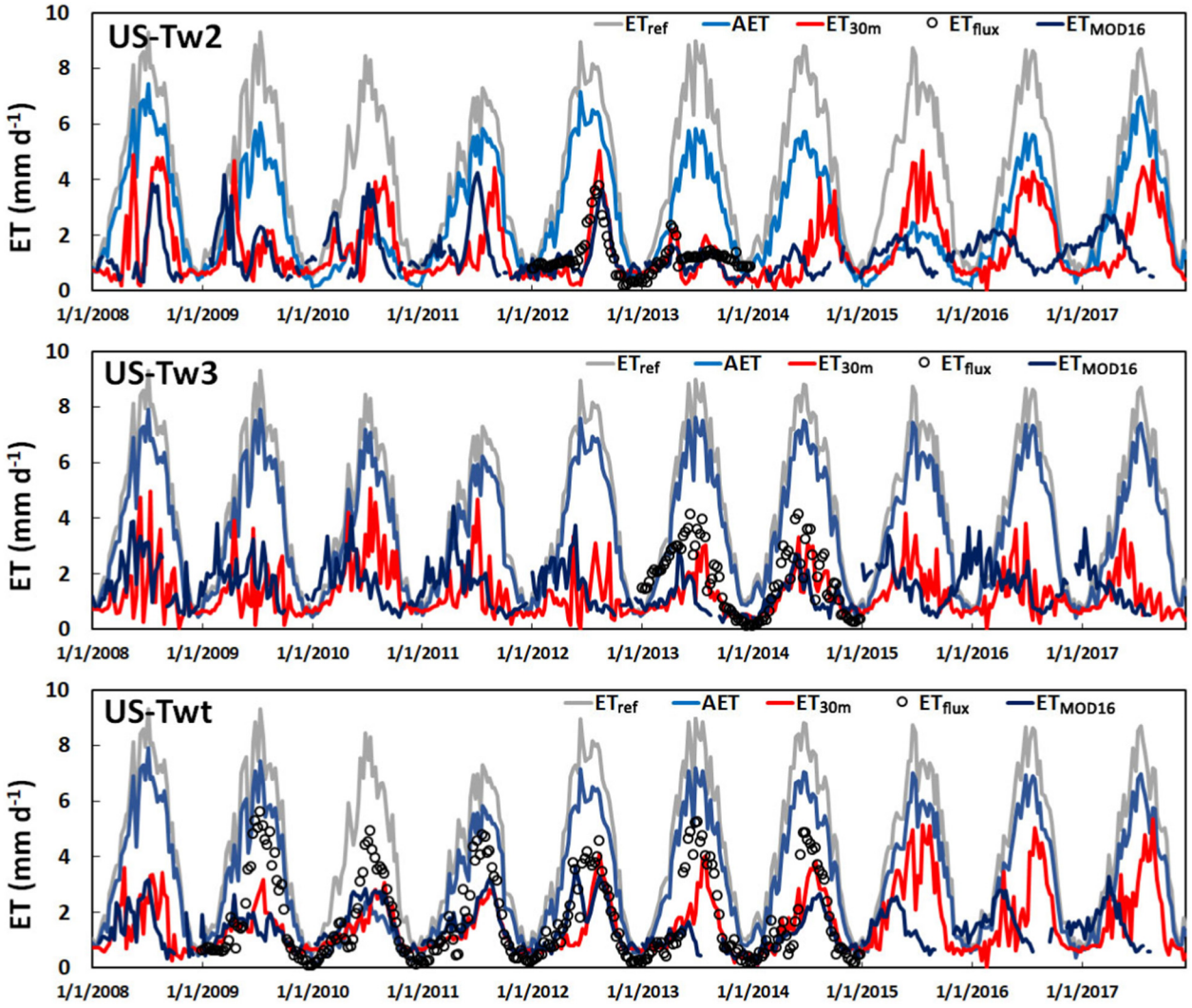

Fig. 4. Seasonal variations of reference ET (ET_{ref}), actual ET derived from ET_{ref} (AET), MODIS MOD16A2 ET (ET_{MOD16}) and finer 30-m ET estimates derived from this study (ET_{30m}) for three cropland flux tower sites (US-Tw2, US-Tw3 and US-Twt) within a California cropland sub-region (ROI1) from 2008 to 2017.

dry conditions and lower in more humid conditions within the semi-arid to sub-humid ($0.20 \leq AI \leq 0.65$) ROI2 domain. The spatial mean of annual ET_{30m} in ROI2 also exhibits higher values under drier conditions and lower values in more humid conditions (Fig. 8); this pattern contrasts with a weak increasing trend ($r = 0.51$; $p = 0.14$) in the ROI2 annual ET_{MOD16} results under more humid conditions.

Many CONUS croplands undergo periodic crop rotations, changing crop type, area and ultimately cropland ET over time. The NASS cropland area in ROI2 fluctuates during the study period and shows a significant ($r = 0.92$; $p < 0.05$) increasing trend of $2.65*10^3$ ha yr^{-1}, ranging from a low of $2.34*10^5$ ha in 2010 to a peak of $2.60*10^5$ ha in 2017 (Fig. 7a). Annual cropland variability depicted from the NASS CDL and the resulting spatial mean values of the annual ET_{30m} results for C3 and C4 crops is shown for ROI2 over the 2008–2017 record (Fig. 7b). The ET_{30m} results in this region show similar ET inter-annual variability between C3 and C4 crop types, with the highest and lowest ET rates in 2012 and 2014, respectively (Fig. 7b). No apparent ET trends are indicted for ether C3 or C4 crop types, though the C4 crops show 3% larger ET interannual variability and 4% larger annual ET_{30m} in this region. C4 crops show a stronger increasing trend (1780 ha yr^{-1}; $p < 0.05$) in cropland area than C3 crops (870 ha yr^{-1}; $p = 0.21$), making a larger (11%) contribution to the observed increase in total cropland area in ROI2. C3 and C4 crops represent about 89% and 94% of the inter-annual variation in total cropland ET (ET_{30m}) in ROI2, respectively. These results imply that the representation of C3 and C4 crop types is a prerequisite for more accurate model ET assessments of heterogeneous croplands, especially at field scale.

4. Discussion

The satellite based ET_{30m} results from this study encompass all CONUS croplands defined from USDA NASS annual cropland classifications and are derived using 30 m 8-day vegetation (EVI) and 4 km daily meteorological inputs using model parameters optimized for C3 and C4 crop types. The ET_{30m} results from this study explained about 64% of the variance in ET_{flux} observations across seven diverse CONUS cropland tower sites, which is comparable with the North American Land Data Assimilation System project phase 2 (NLDAS-2) estimated ET performance for six CONUS cropland tower sites (Xia et al., 2015). The Surface Energy Balance Algorithm for Land (SEBAL) showed relative ET biases of 21% ~ 24% and −15% ~ −30% in California maize and rice fields (Biggs et al., 2016); whereas our results show improved ET_{30m} relative biases of −8.6% and −23% over California maize and rice fields, respectively. The ET_{30m} results also exhibit higher correspondence ($R^2 = 0.86$–0.91) with the ET_{flux} observations at the US-Ne1, US-Ne2 and US-Ne3 sites, which is similar to the reported accuracy attained from the SEBAL and SEBS ET models at these same sites (Singh and Senay, 2015).

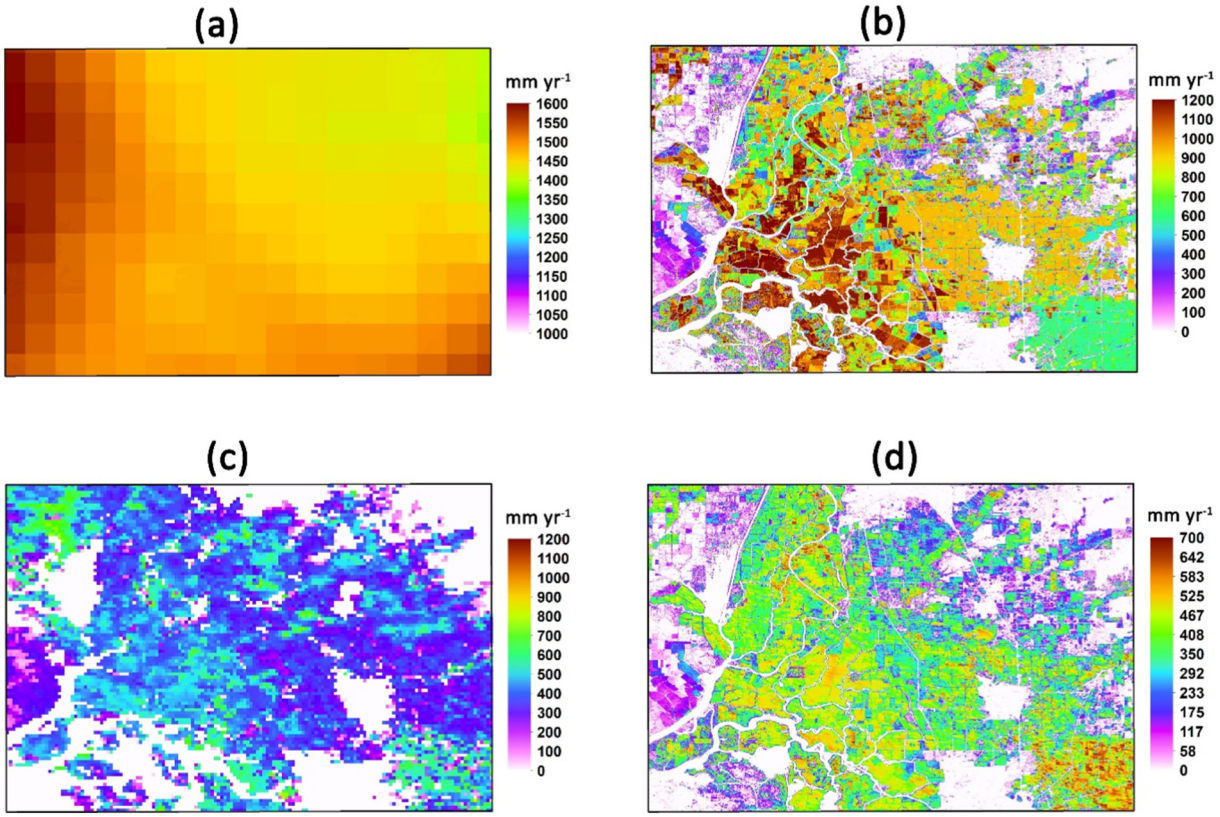

Fig. 5. Spatial patterns of mean annual reference ET (ET_{ref}, a), actual cropland ET derived from ET_{ref} (AET, b) using crop-specific Kc values, MODIS MOD16A2 for cropland (ET_{MOD16}, c) and 30-m cropland ET estimates derived from this study (ET_{30m}, d) for the California sub-region (ROI1) during the 2008–2017 study period.

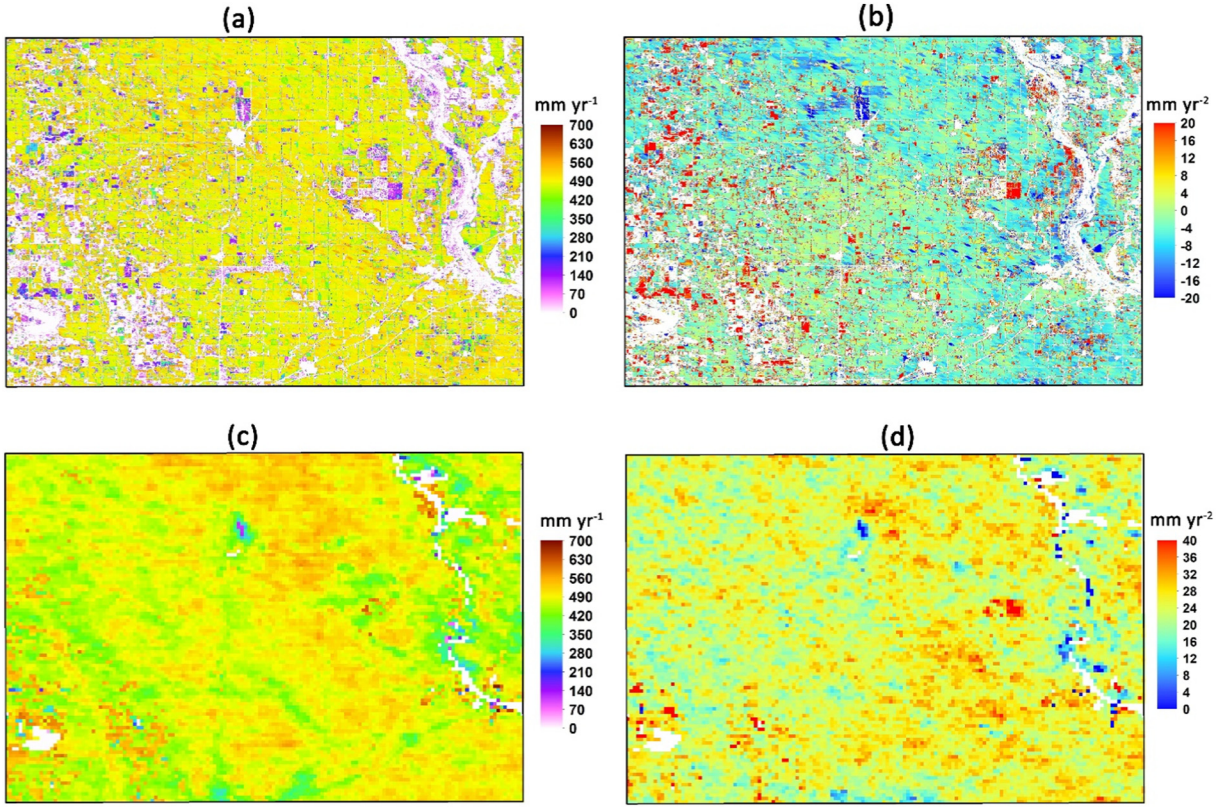

Fig. 6. Spatial distributions of mean annual 30-m cropland ET estimates derived from this study (ET_{30m}, a) and the 500-m MODIS MOD16A2 ET product (ET_{MOD16}, c) for the selected Nebraska cropland sub-region (ROI2) and 2008–2017 study period; the associated temporal trends in annual ET_{30m} (b) and ET_{MOD16} (d) are also shown.

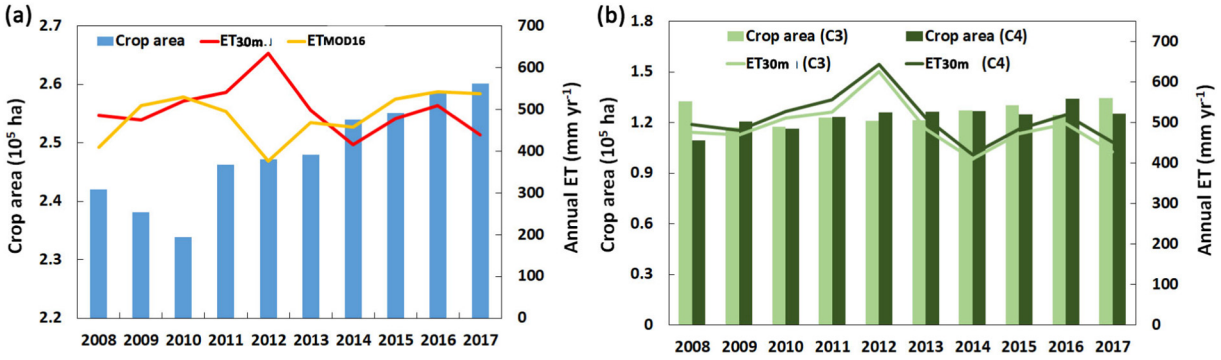

Fig. 7. (a) Annual variations in cropland area, annual 30-m cropland ET estimates derived from this study (ET_{30m}) and the MODIS MOD16A2 product (ET_{MOD16}) for the Nebraska sub-region (ROI2) and 2008–2017 study period; (b) Annual variations of C3 and C4 crop areas in ROI2 defined from the NASS CDL, along with the associated regional mean values of annual ET_{30m} over the period are also shown.

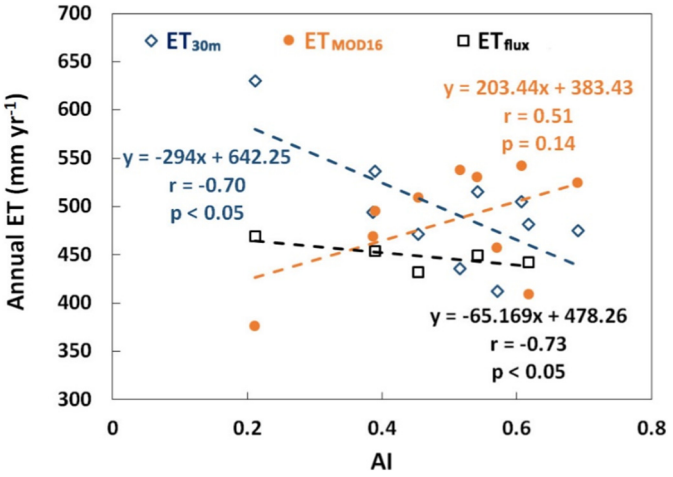

Fig. 8. Correlations between climate aridity index (AI) and mean annual ET_{flux} from 2008 to 2014 for three Nebraska flux tower sites (US-Ne1, US-Ne2 and US-Ne3); the ROI2 spatial mean annual ET estimates derived from this study (ET_{30m}), and the MODIS MOD16A2 product (ET_{MOD16}) are also shown for the same period.

The sensitivity of the ET simulations to regional climate variability within two different CONUS sub-regions over the 10-year (2008–2017) study period was explored in this study. The 30-m and 8-day cropland ET estimates using the MOD16 ET algorithm with the updated BPLUT (ET_{30m}) were strongly correlated with air temperature (T) and vapor pressure deficit (VPD) over the Nebraska sub-region (ROI2), respectively accounting for 67% and 62% of cropland ET variability, and indicating that T and VPD are major contributing factors influencing ET variations in this semi-arid to sub-humid region. For the California sub-region (ROI1), the ET_{30m} results showed lower, but moderate correspondence with T and VPD (R^2 = 0.40 and 0.30, respectively), suggesting that T and VPD still have a significant impact on cropland water losses under the drier climate conditions.

The favorable ET_{30m} performance was largely attributed to the improved model delineation of cropland heterogeneity from the finer (30 m) vegetation (EVI) and land cover (NASS CDL) inputs, and model crop type (C3, C4) calibrations (Figs. 5, 6). However, the above results also highlight the potential impact of the meteorological inputs on model ET error (Wu et al., 2017; Zhao et al., 2006). The MOD16A2 (v6) ET product (ET_{MOD16}) uses relatively coarse (~ 0.5°) resolution global daily meteorological inputs, limiting model performance in heterogeneous regions (Khan et al., 2018; Wang et al., 2015). In this investigation, much finer (4-km) resolution daily meteorology from the CONUS Gridmet record provided the inputs for the model ET_{30m} calculations, providing > 12-fold improved resolution in surface meteorology over the global product, and with favorable regional accuracy (Abatzoglou, 2013). The enhanced meteorological inputs likely contributed to the improved ET_{30m} accuracy relative to the MOD16A2 global ET product (Running et al., 2018), though the 4-km Gridmet data may still be too coarse to capture field scale (30-m) meteorological heterogeneity, including the effects of irrigation and other land management practices (Abatzoglou, 2013; Blankenau, 2017). Further study is needed to fully distinguish the component contributions of the various inputs to the model ET_{30m} performance.

The 30 m EVI record used for the ET_{30m} calculations in this study was produced using an empirical linear regression approach across the CONUS cropland domain and 2008–2017 study period by combining similar spectral information from Landsat (5 and 7) and overlapping MODIS data. A similar Landsat-MODIS data fusion approach was successfully used to generate a 30-m NDVI (normalized difference vegetation index) record for estimating CONUS cropland productivity (He et al., 2018). The EVI records from Landsat (5 and 7) and MODIS show favorable correspondence over both ROI1 ($r = 0.59 \pm 0.24$; $p < 0.05$) and ROI2 ($r = 0.90 \pm 0.12$; $p < 0.05$) during the study period, supporting the underlying assumption of similar overlapping spectral vegetation information from both sensors. The EVI record was used in the MOD16 algorithm to determine available radiant energy and vegetation, and soil contributions to ET. While the empirical EVI downscaling approach used in this study is suitable for our MOD16 ET agricultural application, the vegetation signal may be degraded over complex landscapes due to different sensor footprints and view geometry, and timing of observations (Gao et al., 2017; Ju and Roy, 2008; Robinson et al., 2017). Uncertainties in the fused EVI record can therefore propagate into spatial and temporal errors in the resulting ET record, particularly where Landsat observations are sparse or the spatial scale of EVI variability is below the 500-m MODIS footprint.

An enhanced calibration for C3 and C4 croplands was used to derive ET_{30m} using the MOD16 ET algorithm. However, the model was calibrated and validated against ET_{flux} observations from only a small number of available CONUS cropland tower sites, which may limit model performance over other regions and crop types. Further model refinements, including more detailed calibrations for different crop types, may benefit from additional cropland tower site records potentially available from the global FLUXNET database (Baldocchi et al., 2015). Additionally, the tower ET_{flux} estimates used for the model validation represent a 100–2000 m sampling footprint (Schmid, 1994), which is too coarse for resolving finer spatial heterogeneity at the level of the ET_{30m} model calculations. Although tower observations have been successfully used for model ET calibration and validation in prior studies (e.g. Senay et al., 2016; Yang et al., 2017), finer resolution water flux measurements (e.g. lysimeters) would enable more precise model assessments, but these data are generally unavailable over large regional extents.

While the ET_{30m} results appear to provide for effective ET monitoring over heterogeneous croplands and represent a significant improvement over the other ET records examined in this study, there are several remaining limitations. First, while spatial and annual variations in crop type are represented in the ET_{30m} record from the NASS CDL, other management practices such as the degree of irrigation are not directly represented in the model. AET is expected to approach ET_{ref} under active irrigation and likely contributes significant uncertainty to the ET_{30m} calculations, particularly under strengthening atmospheric moisture deficits during the growing season. Spatial information on irrigated lands and irrigation treatments are expected to further improve the accuracy of the cropland ET calculations.

Another source of ET_{30m} uncertainty is the NASS CDL, which is used in the model to define annual variability in crop type and cropland area across the domain. The 30-m CDL product is generated using relatively fine-scale satellite imagery and an empirical decision-tree classifier, while CDL accuracy is spatially and temporally variable. For example, the reported CDL accuracy during the 2008–2017 study period ranged from 74.7% (2010) to 92.5% (2017) for California and from 89.0% (2017) to 96.4% (2016) for Nebraska. The CDL accuracy may be inflated because it does not account for edge effects (Lark et al., 2017) and may also be lower in regions with complex or sparse agriculture (Larsen et al., 2015). For example, the US-Twt California tower site represents paddy rice over the 2009–2014 period overlapping with this study (Baldocchi et al., 2016). However, the US-Twt site is classified as rice only for 2010, and maize for the other years of record according to the CDL; the resulting crop classification error contributes to the resulting ET_{flux} and ET_{30m} discrepancy at this site (Fig. 4). All of the above factors contribute to uncertainty in the resulting ET_{30m} estimates, which can degrade the ability of the model record to detect climate and land use related ET trends.

The MOD16 algorithm does not directly represent soil moisture related water supply constraints to ET, which may contribute significant model uncertainty, particularly at finer spatial and temporal scales where soil and atmospheric moisture conditions may be uncorrelated (Novick et al., 2016). Crops take water from soil through their root system in order to meet atmospheric moisture demands through transpiration, regulated by canopy stomatal control; ET is therefore strongly sensitive to soil moisture variability (De Lannoy et al., 2006; Sun et al., 2013). Global soil moisture observations are now routinely collected from operational satellite microwave sensors, including the NASA SMAP (Soil Moisture Active Passive) mission which provides enhanced L-band microwave sensitivity to soil moisture with 1–3-day temporal fidelity but at coarse (9–36 km) spatial resolution (Colliander et al., 2017; Reichle et al., 2017). Despite the coarse footprint, the SMAP observations are sensitive to cropland soil moisture and irrigation (Lawston et al., 2017), and have been found to improve the performance of satellite based ET assessments (Purdy et al., 2018). Similar satellite soil moisture observations may further improve MOD16 ET performance, especially in water-limited regions. Adding daily precipitation into the MOD16 algorithm could also improve the model performance, since daily precipitation is the driving factor of daily soil water balance, especially at local scales (Rodriguez-Iturbe, 2000). Thus, more sophisticated approaches may be needed for more precise delineations of climate related impacts affecting ET modeling and trends. Despite the above limitations, the MOD16 algorithm provides an effective framework for field scale cropland ET monitoring based on the well-known Penman-Monteith logic, and directly traceable to the NASA MODIS MOD16A2 operational global ET product. MOD16 also provides a flexible framework for further refinements to improve model performance and utility for agricultural water management and policy applications.

5. Conclusion

This study improves the delineation of field scale (30-m) ET dynamics over CONUS croplands using a satellite-based modeling framework similar to the MODIS MOD16A2 global operational ET product. We used a refined MOD16 algorithm logic calibrated for C3 and C4 crop types, along with enhanced model inputs including 30-m vegetation (EVI) and dynamic cropland cover (NASS CDL), and 4-km daily surface meteorology (Gridmet). The resulting 30-m 8-day MOD16 cropland ET calculations (ET_{30m}) showed favorable performance against ET observations (ET_{flux}) from seven CONUS cropland flux tower sites (R^2 = 0.69; relative RMSE = 53%; relative bias = 3%). The ET_{30m} results also showed better performance than alternative ET estimates from the MODIS MOD16A2 global product (ET_{MOD16}) and MOD16 calculations derived using finer (4-km) meteorological inputs but parameterized for only a single global cropland biome type (ET_{sim}). Relative to ET_{MOD16} and ET_{sim}, the ET_{30m} results exhibited respective 8% and 29% enhancements in R^2 correspondence, 9% reductions in RMSE, and 22% and 8% smaller relative biases in capturing ET_{flux} seasonal dynamics over the cropland tower sites. More traditional cropland ET (AET) derived from 4-km reference ET (ET_{ref}) estimates and crop specific coefficients (Kc) accounted for approximately 52% of the observed ET_{flux} variability at the tower sites but with relatively large overestimation (~ 135%) and degraded performance relative to the ET_{30m} results. The new fine resolution ET product is effective in representing field scale cropland ET heterogeneity, crop type differences and seasonal to inter-annual variability across a diverse range of climate and cropland conditions within the CONUS domain. This heterogeneity is greatly reduced or missing from the coarser 500-m ET_{MOD16} global product.

Acknowledgements

This study was funded by USDA NIFA-AFRI and NASA programs (658 2016-67026-25067, NNX14AI50G, NNX14A169G, 80NSSC18K0738, NNX08AG87A). This work used eddy covariance data acquired and shared by the FLUXNET community, including the AmeriFlux network. The MODIS Collection 6 MOD16A2, MCD43A3 and MCD12Q1 products were retrieved from the online Data Pool, courtesy of the NASA Land Processes Distributed Active Archive Center (LP DAAC), USGS/Earth Resources Observation and Science (EROS) Center, Sioux Falls, South Dakota, https://lpdaac.usgs.gov/data_access/data_pool. A portion of this research was carried out at the Jet Propulsion Laboratory, California Institute of Technology, under contract with NASA.

References

Abatzoglou, J.T., 2013. Development of gridded surface meteorological data for ecological applications and modelling. Int. J. Climatol. 33, 121–131. https://doi.org/10.1002/joc.3413.

Allen, R.G., Walter, I.A., Elliott, R., Itenfisu, D., Brown, P., Jensen, M.E., Mecham, B., Howell, T.A., Snyder, R., Eching, S., Spofford, T., 2005. Task Committee on Standardization of Reference Evapotranspiration.

Allen, R.G., Tasumi, M., Morse, A., Trezza, R., Wright, J.L., Bastiaanssen, W., Kramber, W., Lorite, I., Robison, C.W., 2007a. Satellite-based energy balance for mapping evapotranspiration with internalized calibration (METRIC)—applications. J. Irrig. Drain. Eng. 133, 395–406. https://doi.org/10.1061/(ASCE)0733-9437(2007)133:4(395).

Allen, R.G., Tasumi, M., Trezza, R., 2007b. Satellite-based energy balance for mapping evapotranspiration with internalized calibration (METRIC)—model. J. Irrig. Drain. Eng. 133, 380–394. https://doi.org/10.1061/(ASCE)0733-9437(2007)133:4(380).

Allen, R.G., Pereira, L.S., Howell, T.A., Jensen, M.E., 2011. Evapotranspiration information reporting: I. factors governing measurement accuracy. Agric. Water Manag. 98, 899–920. https://doi.org/10.1016/j.agwat.2010.12.015.

Allen, R.G., Burnett, B., Kramber, W., Huntington, J., Kjaersgaard, J., Kilic, A., Kelly, C., Trezza, R., 2013. Automated calibration of the METRIC-Landsat evapotranspiration process. JAWRA J. Am. Water Resour. Assoc. 49, 563–576. https://doi.org/10.1111/jawr.12056.

Anderson, M.C., Norman, J.M., Mecikalski, J.R., Otkin, J.A., Kustas, W.P., 2007a. A climatological study of evapotranspiration and moisture stress across the continental United States based on thermal remote sensing: 2. Surface moisture climatology. J. Geophys. Res. 112, D11112. https://doi.org/10.1029/2006JD007507.

Anderson, M.C., Norman, J.M., Mecikalski, J.R., Otkin, J.A., Kustas, W.P., 2007b. A climatological study of evapotranspiration and moisture stress across the continental

United States based on thermal remote sensing: 1. Model formulation. J. Geophys. Res. Atmos. 112. https://doi.org/10.1029/2006JD007506.
Anderson, M.C., Norman, J.M., Kustas, W.P., Houborg, R., Starks, P.J., Agam, N., 2008. A thermal-based remote sensing technique for routine mapping of land-surface carbon, water and energy fluxes from field to regional scales. Remote Sens. Environ. 112, 4227–4241. https://doi.org/10.1016/j.rse.2008.07.009.
Anderson, M.C., Kustas, W.P., Norman, J.M., Hain, C.R., Mecikalski, J.R., Schultz, L., González-Dugo, M.P., Cammalleri, C., D'Urso, G., Pimstein, A., Gao, F., 2011. Mapping daily evapotranspiration at field to continental scales using geostationary and polar orbiting satellite imagery. Hydrol. Earth Syst. Sci. 15, 223–239. https://doi.org/10.5194/hess-15-223-2011.
Baldocchi, D.D., 2003. Assessing the eddy covariance technique for evaluating carbon dioxide exchange rates of ecosystems: past, present and future. Glob. Chang. Biol. 9, 479–492. https://doi.org/10.1046/j.1365-2486.2003.00629.x.
Baldocchi, D., Falge, E., Gu, L., Olson, R., Hollinger, D., Running, S., Anthoni, P., Bernhofer, C., Davis, K., Evans, R., Fuentes, J., Goldstein, A., Katul, G., Law, B., Lee, X., Malhi, Y., Meyers, T., Munger, W., Oechel, W., Paw, K.T.U., Pilegaard, K., Schmid, H.P., Valentini, R., Verma, S., Vesala, T., Wilson, K., Wofsy, S., 2001. FLUXNET: a new tool to study the temporal and spatial variability of ecosystem-scale carbon dioxide, water vapor, and energy flux densities. Bull. Am. Meteorol. Soc. 82, 2415–2434. https://doi.org/10.1175/1520-0477(2001)082<2415:fantts>2.3.co;2.
Baldocchi, D., Sturtevant, C., Contributors, F., 2015. Does day and night sampling reduce spurious correlation between canopy photosynthesis and ecosystem respiration? Agric. For. Meteorol. 207, 117–126. https://doi.org/10.1016/j.agrformet.2015.03.010.
Baldocchi, D., Knox, S., Dronova, I., Verfaillie, J., Oikawa, P., Sturtevant, C., Matthes, J.H., Detto, M., 2016. The impact of expanding flooded land area on the annual evaporation of rice. Agric. For. Meteorol. 223, 181–193. https://doi.org/10.1016/j.agrformet.2016.04.001.
Biggs, T.W., Marshall, M., Messina, A., 2016. Mapping daily and seasonal evapotranspiration from irrigated crops using global climate grids and satellite imagery: automation and methods comparison. Water Resour. Res. 52, 7311–7326. https://doi.org/10.1002/2016WR019107.
Blankenau, P.A., 2017. Bias and Other Error in Gridded Weather Data Sets and Their Impacts on Estimating Reference Evapotranspiration. University of Nebraska-Lincoln.
Cheng, L., Xu, Z., Wang, D., Cai, X., 2011. Assessing interannual variability of evapotranspiration at the catchment scale using satellite-based evapotranspiration data sets. Water Resour. Res. 47. https://doi.org/10.1029/2011WR010636.
Colliander, A., Jackson, T.J., Bindlish, R., Chan, S., Das, N., Kim, S.B., Cosh, M.H., Dunbar, R.S., Dang, L., Pashaian, L., Asanuma, J., Aida, K., Berg, A., Rowlandson, T., Bosch, D., Caldwell, T., Caylor, K., Goodrich, D., al Jassar, H., Lopez-Baeza, E., Martínez-Fernández, J., González-Zamora, A., Livingston, S., McNairn, H., Pacheco, A., Moghaddam, M., Montzka, C., Notarnicola, C., Niedrist, G., Pellarin, T., Prueger, J., Pulliainen, J., Rautiainen, K., Ramos, J., Seyfried, M., Starks, P., Su, Z., Zeng, Y., van der Velde, R., Thibeault, M., Dorigo, W., Vreugdenhil, M., Walker, J.P., Wu, X., Monerris, A., O'Neill, P.E., Entekhabi, D., Njoku, E.G., Yueh, S., 2017. Validation of SMAP surface soil moisture products with core validation sites. Remote Sens. Environ. 191, 215–231. https://doi.org/10.1016/j.rse.2017.01.021.
De Lannoy, G.J.M., Verhoest, N.E.C., Houser, P.R., Gish, T.J., Van Meirvenne, M., 2006. Spatial and temporal characteristics of soil moisture in an intensively monitored agricultural field (OPE3). J. Hydrol. 331, 719–730. https://doi.org/10.1016/j.jhydrol.2006.06.016.
Feng, F., Li, X., Yao, Y., Liu, M., 2017. Long-term spatial distributions and trends of the latent heat fluxes over the global cropland ecosystem using multiple satellite-based models. PLoS One 12, e0183771. https://doi.org/10.1371/journal.pone.0183771.
Fischer, M.L., Billesbach, D.P., Berry, J.A., Riley, W.J., Torn, M.S., 2007. Spatiotemporal variations in growing season exchanges of CO 2 , H 2 O, and sensible heat in agricultural fields of the Southern Great Plains. Earth Interact. 11, 1–21. https://doi.org/10.1175/EI231.1.
Fisher, J.B., Tu, K.P., Baldocchi, D.D., 2008. Global estimates of the land–atmosphere water flux based on monthly AVHRR and ISLSCP-II data, validated at 16 FLUXNET sites. Remote Sens. Environ. 112, 901–919. https://doi.org/10.1016/j.rse.2007.06.025.
Friedl, M., Sulla-Menashe, D., 2015. MCD12Q1 MODIS/Terra + Aqua land cover type yearly L3 global 500m SIN grid V006 [data set]. In: NASA EOSDIS Land Processes DAAC, https://doi.org/10.5067/MODIS/MCD12Q1.006.
Gao, F., Anderson, M.C., Zhang, X., Yang, Z., Alfieri, J.G., Kustas, W.P., Mueller, R., Johnson, D.M., Prueger, J.H., 2017. Toward mapping crop progress at field scales through fusion of Landsat and MODIS imagery. Remote Sens. Environ. 188, 9–25. https://doi.org/10.1016/j.rse.2016.11.004.
Gowda, P.H., Senay, G.B., Howell, T.A., Marek, T.H., 2009. Lysimetric evaluation of simplified surface energy balance approach in the Texas high plains. Appl. Eng. Agric. 25, 665–669.
He, M., Kimball, J., Maneta, M., Maxwell, B., Moreno, A., Beguería, S., Wu, X., 2018. Regional crop gross primary productivity and yield estimation using fused Landsat-MODIS data. Remote Sens. 10, 372. https://doi.org/10.3390/rs10030372.
Huete, A.R., Liu, H.Q., Batchily, K., van Leeuwen, W., 1997. A comparison of vegetation indices over a global set of TM images for EOS-MODIS. Remote Sens. Environ. 59, 440–451. https://doi.org/10.1016/S0034-4257(96)00112-5.
Jensen, M.E., Burman, R.D., Allen, R.G., 1990. Evapotranspiration and Irrigation Water Requirements. American Society of Civil Engineers, New York.
Jiang, C., Ryu, Y., 2016. Multi-scale evaluation of global gross primary productivity and evapotranspiration products derived from Breathing Earth System Simulator (BESS). Remote Sens. Environ. 186, 528–547. https://doi.org/10.1016/j.rse.2016.08.030.
Ju, J., Roy, D.P., 2008. The availability of cloud-free Landsat ETM+ data over the conterminous United States and globally. Remote Sens. Environ. 112, 1196–1211. https://doi.org/10.1016/j.rse.2007.08.011.
Jung, M., Reichstein, M., Ciais, P., Seneviratne, S.I., Sheffield, J., Goulden, M.L., Bonan, G., Cescatti, A., Chen, J., de Jeu, R., Dolman, A.J., Eugster, W., Gerten, D., Gianelle, D., Gobron, N., Heinke, J., Kimball, J., Law, B.E., Montagnani, L., Mu, Q., Mueller, B., Oleson, K., Papale, D., Richardson, A.D., Roupsard, O., Running, S., Tomelleri, E., Viovy, N., Weber, U., Williams, C., Wood, E., Zaehle, S., Zhang, K., 2010. Recent decline in the global land evapotranspiration trend due to limited moisture supply. Nature 467, 951. https://doi.org/10.1038/nature09396. https://www.nature.com/articles/nature09396#supplementary-information.
Khan, M.S., Liaqat, U.W., Baik, J., Choi, M., 2018. Stand-alone uncertainty characterization of GLEAM, GLDAS and MOD16 evapotranspiration products using an extended triple collocation approach. Agric. For. Meteorol. 252, 256–268. https://doi.org/10.1016/j.agrformet.2018.01.022.
Knox, S.H., Sturtevant, C., Matthes, J.H., Koteen, L., Verfaillie, J., Baldocchi, D., 2015. Agricultural peatland restoration: effects of land-use change on greenhouse gas (CO2 and CH4) fluxes in the Sacramento-San Joaquin Delta. Glob. Chang. Biol. 21, 750–765. https://doi.org/10.1111/gcb.12745.
Lark, T.J., Mueller, R.M., Johnson, D.M., Gibbs, H.K., 2017. Measuring land-use and land-cover change using the U.S. department of agriculture's cropland data layer: cautions and recommendations. Int. J. Appl. Earth Obs. Geoinf. 62, 224–235. https://doi.org/10.1016/j.jag.2017.06.007.
Larsen, A.E., Hendrickson, B.T., Dedeic, N., MacDonald, A.J., 2015. Taken as a given: evaluating the accuracy of remotely sensed crop data in the USA. Agric. Syst. 141, 121–125. https://doi.org/10.1016/j.agsy.2015.10.008.
Lawston, P.M., Santanello, J.A., Kumar, S.V., 2017. Irrigation signals detected from SMAP soil moisture retrievals. Geophys. Res. Lett. 44 11 (811–860), 867. https://doi.org/10.1002/2017GL075733.
Morton, C.G., Huntington, J.L., Pohll, G.M., Allen, R.G., McGwire, K.C., Bassett, S.D., 2013. Assessing calibration uncertainty and automation for estimating evapotranspiration from agricultural areas using METRIC. JAWRA J. Am. Water Resour. Assoc. 49, 549–562. https://doi.org/10.1111/jawr.12054.
Mu, Q., Heinsch, F.A., Zhao, M., Running, S.W., 2007. Development of a global evapotranspiration algorithm based on MODIS and global meteorology data. Remote Sens. Environ. 111, 519–536. https://doi.org/10.1016/j.rse.2007.04.015.
Mu, Q., Zhao, M., Running, S.W., 2011. Improvements to a MODIS global terrestrial evapotranspiration algorithm. Remote Sens. Environ. 115, 1781–1800. https://doi.org/10.1016/j.rse.2011.02.019.
Mu, Q., Zhao, M., Kimball, J.S., McDowell, N.G., Running, S.W., 2013. A remotely sensed global terrestrial drought severity index. Bull. Am. Meteorol. Soc. 94, 83–98. https://doi.org/10.1175/bams-d-11-00213.1.
Mueller, B., Seneviratne, S.I., Jimenez, C., Corti, T., Hirschi, M., Balsamo, G., Ciais, P., Dirmeyer, P., Fisher, J.B., Guo, Z., Jung, M., Maignan, F., McCabe, M.F., Reichle, R., Reichstein, M., Rodell, M., Sheffield, J., Teuling, A.J., Wang, K., Wood, E.F., Zhang, Y., 2011. Evaluation of global observations-based evapotranspiration datasets and IPCC AR4 simulations. Geophys. Res. Lett. 38. https://doi.org/10.1029/2010GL046230.
Mueller, B., Hirschi, M., Jimenez, C., Ciais, P., Dirmeyer, P.A., Dolman, A.J., Fisher, J.B., Jung, M., Ludwig, F., Maignan, F., Miralles, D.G., McCabe, M.F., Reichstein, M., Sheffield, J., Wang, K., Wood, E.F., Zhang, Y., Seneviratne, S.I., 2013. Benchmark products for land evapotranspiration: LandFlux-EVAL multi-data set synthesis. Hydrol. Earth Syst. Sci. 17, 3707–3720. https://doi.org/10.5194/hess-17-3707-2013.
Nishida, K., Nemani, R.R., Glassy, J.M., Running, S.W., 2003. Development of an evapotranspiration index from Aqua/MODIS for monitoring surface moisture status. IEEE Trans. Geosci. Remote Sens. 41, 493–501. https://doi.org/10.1109/tgrs.2003.811744.
Novick, K.A., Ficklin, D.L., Stoy, P.C., Williams, C.A., Bohrer, G., Oishi, A.C., Papuga, S.A., Blanken, P.D., Noormets, A., Sulman, B.N., Scott, R.L., Wang, L., Phillips, R.P., 2016. The increasing importance of atmospheric demand for ecosystem water and carbon fluxes. Nat. Clim. Chang. 6, 1023. https://doi.org/10.1038/nclimate3114. https://www.nature.com/articles/nclimate3114#supplementary-information.
Oikawa, P.Y., Sturtevant, C., Knox, S.H., Verfaillie, J., Huang, Y.W., Baldocchi, D.D., 2017. Revisiting the partitioning of net ecosystem exchange of CO2 into photosynthesis and respiration with simultaneous flux measurements of 13CO2 and CO2, soil respiration and a biophysical model, CANVEG. Agric. For. Meteorol. 234–235, 149–163. https://doi.org/10.1016/j.agrformet.2016.12.016.
Oki, T., Kanae, S., 2006. Global hydrological cycles and world water resources. Science 313, 1068–1072. https://doi.org/10.1126/science.1128845. 80-.
Purdy, A.J., Fisher, J.B., Goulden, M.L., Colliander, A., Halverson, G., Tu, K., Famiglietti, J.S., 2018. SMAP soil moisture improves global evapotranspiration. Remote Sens. Environ. 219, 1–14. https://doi.org/10.1016/j.rse.2018.09.023.
Reichle, R.H., Lannoy, G.J.M. De, Liu, Q., Ardizzone, J.V., Colliander, A., Conaty, A., Crow, W., Jackson, T.J., Jones, L.A., Kimball, J.S., Koster, R.D., Mahanama, S.P., Smith, E.B., Berg, A., Bircher, S., Bosch, D., Caldwell, T.G., Cosh, M., González-Zamora, Á., Collins, C.D.H., Jensen, K.H., Livingston, S., Lopez-Baeza, E., Martínez-Fernández, J., McNairn, H., Moghaddam, M., Pacheco, A., Pellarin, T., Prueger, J., Rowlandson, T., Seyfried, M., Starks, P., Su, Z., Thibeault, M., Velde, R. van der, Walker, J., Wu, X., Zeng, Y., 2017. Assessment of the SMAP Level-4 surface and root-zone soil moisture product using in situ measurements. J. Hydrometeorol. 18, 2621–2645. https://doi.org/10.1175/jhm-d-17-0063.1.
Robinson, N., Allred, B., Jones, M., Moreno, A., Kimball, J., Naugle, D., Erickson, T., Richardson, A., 2017. A dynamic Landsat derived normalized difference vegetation index (NDVI) product for the conterminous United States. Remote Sens. 9, 863.
Rodriguez-Iturbe, I., 2000. Ecohydrology: a hydrologic perspective of climate-soil-vegetation dynamics. Water Resour. Res. https://doi.org/10.1029/1999WR900210.
Running, S.W., Mu, Q., Zhao, M., Moreno, A., 2018. User's Guide: MODIS Global Terrestrial Evapotranspiration (ET) Product (NASA MOD16A2/A3) NASA Earth

Observing System MODIS Land Algorithm. (Washington, DC, USA).
Schaaf, C., Wang, Z., 2015. MCD43A3 MODIS/Terra + Aqua BRDF/Albedo daily L3 global - 500m V006 [data set]. In: NASA EOSDIS Land Processes DAAC, https://doi.org/10.5067/MODIS/MCD43A3.006.
Schmid, H.P., 1994. Source areas for scalars and scalar fluxes. Bound.-Layer Meteorol. 67, 293–318. https://doi.org/10.1007/BF00713146.
Schubert, S.D., Rood, R.B., Pfaendtner, J., 1993. An Assimilated Dataset for Earth Science Applications. Bull. Am. Meteorol. Soc. 74, 2331–2342. https://doi.org/10.1175/1520-0477(1993)074<2331:aadfes>2.0.co;2.
Scott, R.L., Huxman, T.E., Cable, W.L., Emmerich, W.E., 2006. Partitioning of evapotranspiration and its relation to carbon dioxide exchange in a Chihuahuan Desert shrubland. Hydrol. Process. 20, 3227–3243. https://doi.org/10.1002/hyp.6329.
Senay, G.B., Budde, M.E., Verdin, J.P., 2011. Enhancing the simplified surface energy balance (SSEB) approach for estimating landscape ET: validation with the METRIC model. Agric. Water Manag. 98, 606–618. https://doi.org/10.1016/j.agwat.2010.10.014.
Senay, G.B., Friedrichs, M., Singh, R.K., Velpuri, N.M., 2016. Evaluating Landsat 8 evapotranspiration for water use mapping in the Colorado River Basin. Remote Sens. Environ. 185, 171–185. https://doi.org/10.1016/J.RSE.2015.12.043.
Singh, R., Senay, G., 2015. Comparison of four different energy balance models for estimating evapotranspiration in the Midwestern United States. Water 8, 9. https://doi.org/10.3390/w8010009.
Sun, L., Liang, S., Yuan, W., Chen, Z., 2013. Improving a Penman–Monteith evapotranspiration model by incorporating soil moisture control on soil evaporation in semiarid areas. Int. J. Digit. Earth 6, 134–156. https://doi.org/10.1080/17538947.2013.783635.
Suyker, A.E., Verma, S.B., Burba, G.G., Arkebauer, T.J., Walters, D.T., Hubbard, K.G., 2004. Growing season carbon dioxide exchange in irrigated and rainfed maize. Agric. For. Meteorol. 124, 1–13. https://doi.org/10.1016/j.agrformet.2004.01.011.
Suyker, A.E., Verma, S.B., Burba, G.G., Arkebauer, T.J., 2005. Gross primary production and ecosystem respiration of irrigated maize and irrigated soybean during a growing season. Agric. For. Meteorol. 131, 180–190. https://doi.org/10.1016/j.agrformet.2005.05.007.
Tasumi, M., Allen, R.G., 2007. Satellite-based ET mapping to assess variation in ET with timing of crop development. Agric. Water Manag. 88, 54–62. https://doi.org/10.1016/j.agwat.2006.08.010.
UNESCO, n.d. United Nations Educational, Scientific and Cultural Organization (UNESCO), 1979. Map of the World Distribution of Arid Regions: Map at Scale 1:25000000 with Explanatory Note. MAB Technical Notes 7, UNESCO, Paris.
Velpuri, N.M., Senay, G.B., Singh, R.K., Bohms, S., Verdin, J.P., 2013. A comprehensive evaluation of two MODIS evapotranspiration products over the conterminous United States: using point and gridded FLUXNET and water balance ET. Remote Sens. Environ. 139, 35–49. https://doi.org/10.1016/j.rse.2013.07.013.
Vermote, E., 2015. MOD09A1 MODIS/Terra surface reflectance 8-day L3 global 500m SIN grid V006 [data set]. NASA EOSDIS LP DAAC. https://doi.org/10.5067/MODIS/MOD09A1.006.
Vinukollu, R.K., Wood, E.F., Ferguson, C.R., Fisher, J.B., 2011. Global estimates of evapotranspiration for climate studies using multi-sensor remote sensing data: evaluation of three process-based approaches. Remote Sens. Environ. 115, 801–823. https://doi.org/10.1016/j.rse.2010.11.006.
Wang, S., Pan, M., Mu, Q., Shi, X., Mao, J., Brümmer, C., Jassal, R.S., Krishnan, P., Li, J., Black, T.A., 2015. Comparing evapotranspiration from Eddy covariance measurements, water budgets, remote sensing, and land surface models over Canada. J. Hydrometeorol. 16, 1540–1560. https://doi.org/10.1175/jhm-d-14-0189.1.
Wu, Z., Ahlström, A., Smith, B., Ardö, J., Eklundh, L., Fensholt, R., Lehsten, V., 2017. Climate data induced uncertainty in model-based estimations of terrestrial primary productivity. Environ. Res. Lett. 12, 064013. https://doi.org/10.1088/1748-9326/aa6fd8.
Xia, Y., Hobbins, M.T., Mu, Q., Ek, M.B., 2015. Evaluation of NLDAS-2 evapotranspiration against tower flux site observations. Hydrol. Process. 29, 1757–1771. https://doi.org/10.1002/hyp.10299.
Xiong, Y.J., Zhao, S.H., Tian, F., Qiu, G.Y., 2015. An evapotranspiration product for arid regions based on the three-temperature model and thermal remote sensing. J. Hydrol. 530, 392–404. https://doi.org/10.1016/j.jhydrol.2015.09.050.
Xu, C.Y., Singh, V.P., 2005. Evaluation of three complementary relationship evapotranspiration models by water balance approach to estimate actual regional evapotranspiration in different climatic regions. J. Hydrol. 308, 105–121. https://doi.org/10.1016/j.jhydrol.2004.10.024.
Yang, Y., Long, D., Shang, S., 2013. Remote estimation of terrestrial evapotranspiration without using meteorological data. Geophys. Res. Lett. 40, 3026–3030. https://doi.org/10.1002/grl.50450.
Yang, Y., Anderson, M.C., Gao, F., Hain, C.R., Semmens, K.A., Kustas, W.P., Noormets, A., Wynne, R.H., Thomas, V.A., Sun, G., 2017. Daily Landsat-scale evapotranspiration estimation over a forested landscape in North Carolina, USA, using multi-satellite data fusion. Hydrol. Earth Syst. Sci. 21, 1017–1037. https://doi.org/10.5194/hess-21-1017-2017.
Zhang, K., Kimball, J.S., Nemani, R.R., Running, S.W., 2010. A continuous satellite-derived global record of land surface evapotranspiration from 1983 to 2006. Water Resour. Res. 46. https://doi.org/10.1029/2009WR008800.
Zhao, M., Running, S.W., Nemani, R.R., 2006. Sensitivity of moderate resolution imaging spectroradiometer (MODIS) terrestrial primary production to the accuracy of meteorological reanalyses. J. Geophys. Res. Biogeosci. 111. https://doi.org/10.1029/2004JG000004.